# Structure and immunomodulatory property relationship in NapA of Borrelia burgdorferi.

Biochimica et Biophysica Acta 1804 (2010) 2191–2197

Contents lists available at ScienceDirect

Biochimica et Biophysica Acta

journal homepage: www.elsevier.com/locate/bbapap

# Structure and immunomodulatory property relationship in NapA of *Borrelia burgdorferi*☆

Gaia Codolo [a,d], Elena Papinutto [a,b], Alessandra Polenghi [a], Mario Milco D'Elios [c], Giuseppe Zanotti [a,b,*], Marina de Bernard [a,d,*]

[a] Venetian Institute of Molecular Medicine, Via Orus 2, 35129 Padua, Italy
[b] Department of Biological Chemistry, University of Padua, Viale G. Colombo 3, 35131 Padua, Italy
[c] Department of Internal Medicine, University of Florence, Viale Morgagni 85, 50134 Florence, Italy
[d] Department of Biology, University of Padua, Viale G. Colombo 3, 35131 Padua, Italy

ARTICLE INFO

*Article history:*
Received 10 May 2010
Received in revised form 20 August 2010
Accepted 5 September 2010
Available online 19 September 2010

*Keywords:*
Th17
TLR2
Dps-like proteins
Miniferritin
Dodecamer

ABSTRACT

NapA from *Borrelia burgdorferi* is a member of the Dps-like protein family with specific immunomodulatory properties; in particular, NapA is able to induce the expression of IL-23 in neutrophils and monocytes, as well as the expression of IL-6, IL-1β, and transforming growth factor beta (TGF-β) in monocytes, via Toll-like receptor (TLR) 2. Such an activity on innate immune cells triggers a synovial fluid Th17 response. Here we report the crystal structure of NapA, determined at 2.6 Å resolution, which shows that the quaternary structure of the protein is that of a dodecamer with 23 symmetry, typical of the proteins of the family. We also demonstrate that the N- and C-terminal tails, which are flexible and not visible in the crystal, are not relevant for its pro-Th17 activity. Based on the crystal structure and on the comparison with the structure of the orthologous protein from *Helicobacter pylori*, HP-NAP, we hypothesize that the charge distributions on the two proteins' surfaces are responsible for the interaction with TLR2 and for the different behaviors in modulating the immune response.



## 1. Introduction

DNA-protecting proteins (Dps) are a family of bacterial stress proteins, capable of sequestering iron, that are induced under nutrient limitations. Dps-like proteins are widely expressed in prokaryotes [1] but they display different activities in different bacteria [2]. In the last few years we have demonstrated that at least two of them possess immunomodulatory properties and are of great relevance for driving and orchestrating different types of innate and adaptive immune responses; they are HP-NAP of *Helicobacter pylori* and NapA of *Borrelia burgdorferi* [3,4]. HP-NAP, originally defined as neutrophil activating protein because of its ability to stimulate neutrophils to produce oxygen radicals [5], is now considered a crucial factor in driving the T helper (Th) 1 inflammation in *H. pylori* infection [4,6]. NapA was found to be essential for *B. burgdorferi* persistence within ticks [7] but, most importantly, we recently reported that it represents a major target of the humoral response in patients with Lyme arthritis. We also showed that NapA is an important driver of interleukin (IL)-23 and IL-17 immune responses, and elicits a synovial Th17 response that might play an important role in the pathogenesis of Lyme arthritis, a possible clinical outcome of the infection sustained by *B. burgdorferi* [3]. Therefore NapA and HP-NAP, although their sequences are identical to 28% (Fig. 1A), are endowed with different immunological properties, being the former a pro-Th17 agonist and the latter an inducer of Th1-oriented responses.

NapA possesses two peculiarities that might be implicated in its specific immunological activity: it is 13 amino acids longer at the N-terminus and 20 amino acids longer at the C-terminus than HP-NAP from *H. pylori*. On the basis of these differences, we were concerned to verify whether in these two portions of the molecule could reside the unique Th17-orienting property of NapA. Moreover, the fact that synovial fluid-derived NapA-specific T cells of patients with Lyme arthritis produced IL-17, further supported the hypothesis that NapA contains Th17 motifs in its non-conserved parts [3].

Here we describe the crystallographic structure of NapA, which is similar to that of the other members of the Dps-like family. We also demonstrate that the Th17-orienting property of NapA does not reside in its N- and C-terminal tails.

*Abbreviations:* Dps, DNA-protecting proteins; HP-NAP, *Helicobacter pylori* neutrophil activating protein; NapA, Neutrophil activating protein A; TLR, Toll-like receptor

☆ Data deposition: the atomic coordinates and structure factors of NapA have been deposited in the Protein Data Bank, http://www.rcsb.org (PDB ID code 2PYB).

* Corresponding authors. M. de Bernard is to be contacted at Venetian Institute of Molecular Medicine, Via Orus 2, 35129 Padova Italy. Tel.: +39 049 7923223; fax: +39 049 7923250. G. Zanotti, Department of Biological Chemistry, University of Padova, Viale G. Colombo 3, 35131 Padova Italy. Tel.: +39 049 8276409; fax: +39 049 8073310.
*E-mail addresses:* giuseppe.zanotti@unipd.it (G. Zanotti), marina.debernard@unipd.it (M. de Bernard).

1570-9639/$ – see front matter © 2010 Elsevier B.V. All rights reserved.
doi:10.1016/j.bbapap.2010.09.004

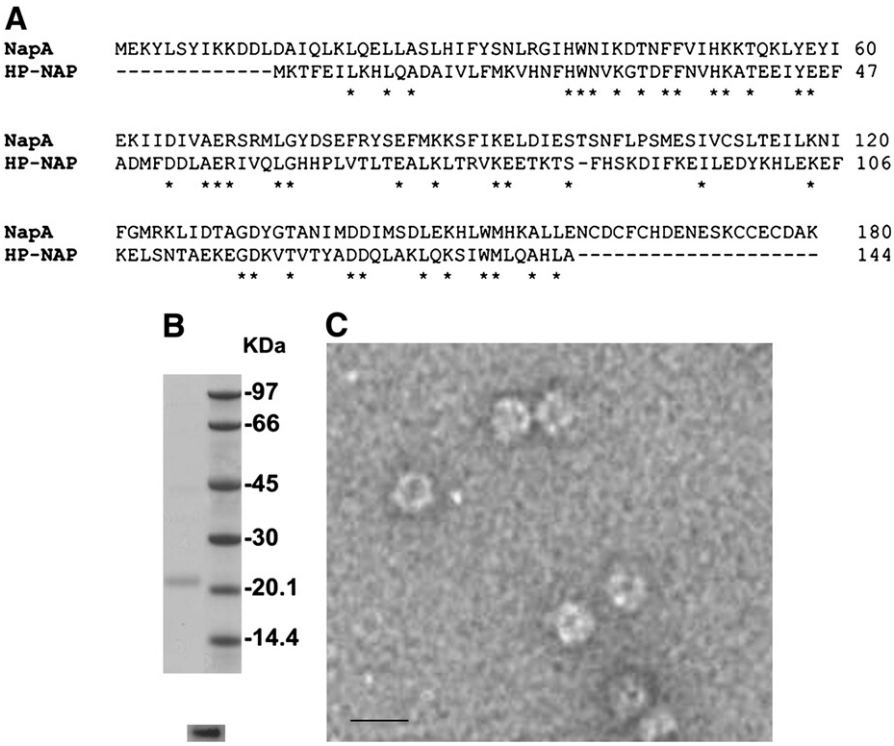


**Fig. 1.** Sequence and purification of NapA. (A) Amino acid sequence alignment between NapA of *Borrelia burgdorferi* and HP-NAP of *Helicobacter pylori*. * indicate the identities between the two sequences. (B) Coomassie blue stained SDS-PAGE of recombinant NapA, purified from *B. subtilis*, reveals the purity of the protein. The identity of NapA was confirmed by using a specific polyclonal antibody in a Western blot analysis (lower box). (C) Electron microscopy analysis of negatively stained NapA. Scale bar, 10 nm.

## 2. Materials and methods

### 2.1. Reagents

The mouse monoclonal blocking antibody against human TLR2 was from Genentech. Polyclonal antibody anti NapA was raised in rabbit using the purified recombinant protein as antigen.

### 2.2. Cloning and protein purification

NapA was cloned, expressed, and purified from *Bacillus subtilis*. The NapA gene was amplified by PCR from *B. burgdorferi* strain B31, using standard methods, with the following primers: 5′-CCCGAGCTCATAAAGGAGATAGTTATG-3′ and 5′-CCCAAGCTTCTATTTTGCATCACACTC-3′. The N-terminal and C-terminal deletion mutants of NapA (abbreviated as ΔN-ter and ΔC-ter in the text) were obtained amplifying by PCR the NapA gene with the following couple of primers: 5′-CCCGAGCTCTATAAAAAAGGATGATTTAATG-3′ and 5′-CCCAAGCTTCTATTTTGCATCACACTC-3′ for the ΔN-ter mutant; and 5′-CCCGAGCTCATAAAGGAGATAGTTATG-3′ and 5′-CCCAAGCTTTTATTCAAGCAATGCCTTATGC-3′ for the ΔC-ter mutant. These primers contain *Sac*I or *Hind*III restriction enzyme sites (underlined). PCR reaction was carried out using standard methods and the thermal cycling parameters were as follows: 95 °C for 15 min followed by 29 cycles of 94 °C (1 min), 50 °C (1 min), 72 °C (1 min) and a final elongation step at 72 °C (5 min) [8]. The amplified fragments were digested with *Sac*I and *Hind*III overnight at 37 °C and ligated into the *Sac*I and *Hind*III sites of the expression vector pSM214G. pSM214G contains an artificial constitutive promoter, a chloramphenicol resistance cassette, and two origins of replication that allow expression of the cloned gene both in *E. coli* and *B. subtilis*.

*B. subtilis* strain SMS 118 containing the plasmid pSM214G-NapA (either wt or mutant) was grown for 15 h in YT medium (15 g/l yeast extract, 16 g/l bactotryptone, 5 g/l NaCl) with 15 μg/ml chloramphenicol. Cells were pelleted by centrifugation at 4,000 *g* and resuspended in 10 ml of Tris–HCl 30 mM, pH 7.8 plus protease inhibitors (Roche). After three passages through a French Press and removal of debris by centrifugation at 32,000 *g*, ammonium sulphate (60% for wt protein and 40% for the mutants) was added to the supernatant and kept for 3 h at 4 °C with slow continuous stirring. At this percentage of ammonium sulphate most of the protein NapA remained in solution. The solution was centrifuged at 32,000 *g* and the supernatant was dialyzed overnight in buffer A (Tris–HCl 30 mM, pH 7.8, NaCl 0.1 M) and then loaded onto an anion exchange pre-packed column (MonoQ FPLC, GE Healthcare) equilibrated with the same buffer. Using a linear gradient from 0.1 to 0.4 M NaCl in buffer A, NapA was eluted in a range from 0.41 to 0.51 M NaCl. The fractions containing the protein were pooled and DTT was added to a final concentration of 10 mM. NapA was further purified by gel filtration chromatography (Superdex200 HR 10/30, GE Healthcare) with phosphate buffer, pH 7.8, DTT 10 mM. Protein was concentrated using the ultrafiltration system Centricon® (Millipore), and the final product was checked for purity in a Coomassie brilliant blue stained gel and analyzed by western blot with a specific polyclonal antibody.

### 2.3. Electron microscopy and iron detection

One drop (10 μl) of wt NapA 50 μg/ml in phosphate buffer was placed on a thin carbon film supported by a copper grid. Unbuffered 1% uranyl acetate was used as a negative stain. Micrographs were taken with a Hitachi H-600 electron microscope at a magnification of 40,000× and recorded on SO-163 Kodak film. The presence of iron into the molecule was detected using the Fe(II) 2,2′bypiridyl method [9]. 0.1 mg of purified protein was treated with sodium dithionite (0.3% w/v) to reduce possible Fe(III) to Fe(II); subsequently a 50 mM solution of 2,2′-bypiridyl was added to chelate ferrous iron. The amount of iron was estimated by spectrophotometric measurements at 520 nm (Perkin Elmer). At this wavelength, the complex $[Fe(II)(2,2'bypiridyl)3]^{2+}$ has a maximum of absorbance.

### 2.4. Crystallization, data collections and processing

Crystallization trials were performed with the hanging drop vapour diffusion technique, by mixing 3 μl drops of the protein sample, at 9 mg/ml in buffer (20 mM $Na_2HPO_4$, pH 6.5, 0.1 M NaCl, 10 mM DTT), with 3 μl of precipitant solution (0.1 M sodium acetate, pH 4.5 and 26–30% MPD). The drop was equilibrated against a 500 μl reservoir of the same precipitant solution (30% MPD). Crystals grew in a few days at 293 K. Diffraction data were measured at the X-ray diffraction beamline of the ELETTRA synchrotron in Trieste (Italy). One crystal, frozen at 100K under a nitrogen gas cold stream without the need of any cryoprotectant solution, allowed the measurement of an entire native data set. A wavelength of 1.2 Å was selected. Diffraction data were measured using an imaging-plate recorder (MAR research, diameter 345 mm). Data were processed with the MOSFLM software [10] and reduced and merged with SCALA [11]. NapA crystals belong to the trigonal R3 space group, with cell parameters: a = b = 93.08 Å and c = 227.50 Å, four monomers per asymmetric unit.

### 2.5. Structure determination and refinement

The structure of *B. burgdorferi* NapA was solved by molecular replacement using the MolRep software of the CCP4 suite [11]. The initial search for the rotation function was performed at 3 Å resolution using a tetramer model of the protein generated automatically by the ExPASy server [12]. A statistical analysis of the observed intensities indicated the presence of merohedral twinning in the crystal, with the twinning law (h,−h−k,−l) and a twinning fraction of about 0.45. All the refinement was carried out using the software package CNS [13], using non-crystallographic restraints among the four monomers. The use of the twinning option during the refinement introduced some instability in the process. For this reason, the model was refined as for a non-twinned crystal, reducing the crystallographic R factor to 0.33 (Rfree = 0.368). At this point, the introduction of the twinning option reduced the R factor to the final value of 0.247 (Rfree = 0.275). Model visualization and rebuilding was performed with the Coot graphic program [14]. Owing to the relatively low resolution, only 33 water molecules were introduced, 8 of them in correspondence to the iron ions to complete the coordination. Only residues from 11 to 161 are visible in the electron density. Statistics on data collection and refinement are reported in Table 1.

The quality of the final model is relatively low, owing both to the relatively low resolution, 2.6 Å, and to the presence of twinning. Nevertheless stereochemistry, as assessed by the PROCHECK program [15], is satisfactory at this resolution: only 2.8% of residues lie in the "generously allowed" and 0.7% (one residue per monomer) in disallowed regions of the Ramachandran plot. The overall G-factor is 0.0.

**Table 1**
Data collection and refinement statistics.

| | |
|---|---|
| *Data collection* | |
| Resolution (Å) | 50–2.6 (2.76–2.6) |
| Space group, cell parameters | R3, a = b = 93.08 Å, c = 227.50 Å |
| Independent reflections | 22,533 (2778) |
| Multiplicity | 2.8 (2.8) |
| Completeness (%) | 99.7 (99.9) |
| $\langle I/\sigma(I)\rangle$ | 6.4 (1.3) |
| $R_{merge}$ | 0.075 (0.388) |
| *Refinement* | |
| Protein atoms | 4984 |
| Solvent molecules/Fe atoms | 24/8 |
| $R_{cryst.}$ | 0.242 (0.405) |
| $R_{free}$ | 0.275 (0.451) |
| R.m.s. on bond distances (Å) | 0.014 |
| R.m.s. on bond angles (°) | 1.8 |

Numbers in parentheses refer to the last resolution shell. $R_{free}$ was calculated with 7% of the data. A wavelength of 1.2 Å was used.

### 2.6. Coordinates

Atomic coordinates and structure factors (codes 2PYB) have been deposited in the Protein Data Bank, Research Collaboratory for Structural Bioinformatics, Rutgers University, New Brunswick, NJ (http://www.rcsb.org/).

### 2.7. Preparation of monocytes

Human monocytes were prepared from healthy donors as described [16]. Monocytes were cultured in RPMI-1640 10% FCS in the presence of 1 μM of NapA, NapA ΔN-ter, or NapA ΔC-ter; NapA vehicle (PBS) was applied as control. When required, cells were preincubated 2 h with 20 μg/ml of anti-TLR2 blocking antibody before stimuli exposure.

### 2.8. Real time PCR analysis

Total RNA was isolated from $2 \times 10^6$ monocytes using TriZOL solution (Invitrogen) according to the manufacturer's instructions. RNA was reverse-transcribed and amplified with the following primers: 5′-AGCAACAGGGTGGTGGAC-3′ and 5′-GTGTGGTGGGGGACTGAG-3′ for GAPDH; 5′-TCCACCAGGGTCTGATTTTT-3′ and 5′-TTGAAGCGGA-GAAGGAGACG-3′ for IL-23p19; 5′-ACAAAGGAGGCGAGGTTCTAA-3′ and 5′-CCCTTGGGGGTCAGAAGAG-3′ for IL-12p40; 5′-AACCT-GAACCTTCCAAAGATGG-3′ and 5′-TCTGGCTTGTTCCTCACTACT-3′ for IL-6; 5′-CTGTCCTGCGTGTTGAAAGA-3′ and 5′- TTGGGT-AATTTTTGGGATCTACA-3′ for IL-1β; 5′-AGTGGTTGAGCCGTGGAG-3′ and 5′-CCATGAGAAGCAGGAAAGG-3′ for TGF-β. After the amplification, data analysis was performed using the second derivative method algorithm. For each sample, the amount of cytokine mRNA (IL-23p19, IL-12p40, IL-6, IL-1β and TGF-β) was expressed as *n* fold of the normalized amount of mRNA from untreated cells (1 AU = mRNA cytokine concentration [fmol/μl]/mRNA GAPDH [fmol/μl]).

### 2.9. Detection of cytokines in monocyte culture supernatants

Culture supernatants of monocytes, harvested for mRNA quantification, were collected and the amounts of IL-23, TGF-β, IL-6 and IL-1β were quantified by ELISA according to the manufacturer's instructions (BioSource International for IL-23, TGF-β and IL-6 and Biolegend for IL-1β).

### 2.10. Statistical analysis

Data were expressed as mean values ± SD. Statistical significance between different groups of mice was calculated by unpaired Student's t-test. A probability (p) of less than 0.05 was considered significant.

## 3. Results

### 3.1. Structure of the monomer

The gene encoding NapA was cloned and expressed in *B. subtilis*. The final product was checked for purity in a Coomassie brilliant blue stained gel and analyzed by western blot with a specific polyclonal antibody (Fig. 1B). The dimensions of the oligomers formed by ferritins and proteins of the Dps family are such that they can be studied at a low resolution by electron microscopy. Electron micrograph of negatively stained samples of NapA (Fig. 1C) clearly shows that it forms oligomers with a central cavity, a structure

reminiscent of those of other Dps-like proteins [1]. To gain more detailed information about the structural organization of NapA, the recombinant protein was crystallized and its structure determined by X-ray diffraction at 2.6 Å resolution. The NapA monomer (Fig. 2A) was found to adopt the typical folding of the Dps-like family members [1,17–19] characterized by a four-helix bundle. Helices A (residues from 15 to 40) and B (from 46 to 53) are connected through a long strand to helices C (residues from 113 to 127) and D (residues from 133 to 153). Another short piece of helix, quite distorted in our model (residues 82–88), is present in the center of the long strand that connects the first two to the last two helices. Superposition of the Cα chain trace of NapA monomer with that of other bacterial mini-ferritins gives root mean square values ranging from 1.4 to 1.8 Å. The major significant difference is represented by a turn (residues from 102 to 107) present at the beginning of α-helix C, since the presence of a Pro residue in position 104 prevents the formation of the α-helix. Other differences can be observed at the N- and C-terminus. In particular, NapA has a longer N-terminal (about 10 residues) and C-terminal tail (about 19 residues) with respect to most of the other members of the family. Both the N- and C-terminus extensions cannot be seen in the electron density map, indicating that they are flexible and/or disordered. The C-terminus is rich in cysteine residues (6 Cys in 19 residues), but the electron density map for our model stops at residue 161, and only Cys 160 is visible. A possible explanation could be that the protein, during purification and crystallization, was permanently kept in the presence of 10 mM DTT. These conditions were selected in order to avoid the formation of intermolecular disulfide bridges between the Cys residues exposed on the protein surface, since the presence of covalent dimers was observed during the purification process of the protein. At the same time, the use of reducing conditions could have hindered a correct folding of the C-terminal part of each monomer, since the eventual correct formation of the S–S bridges was also hindered.

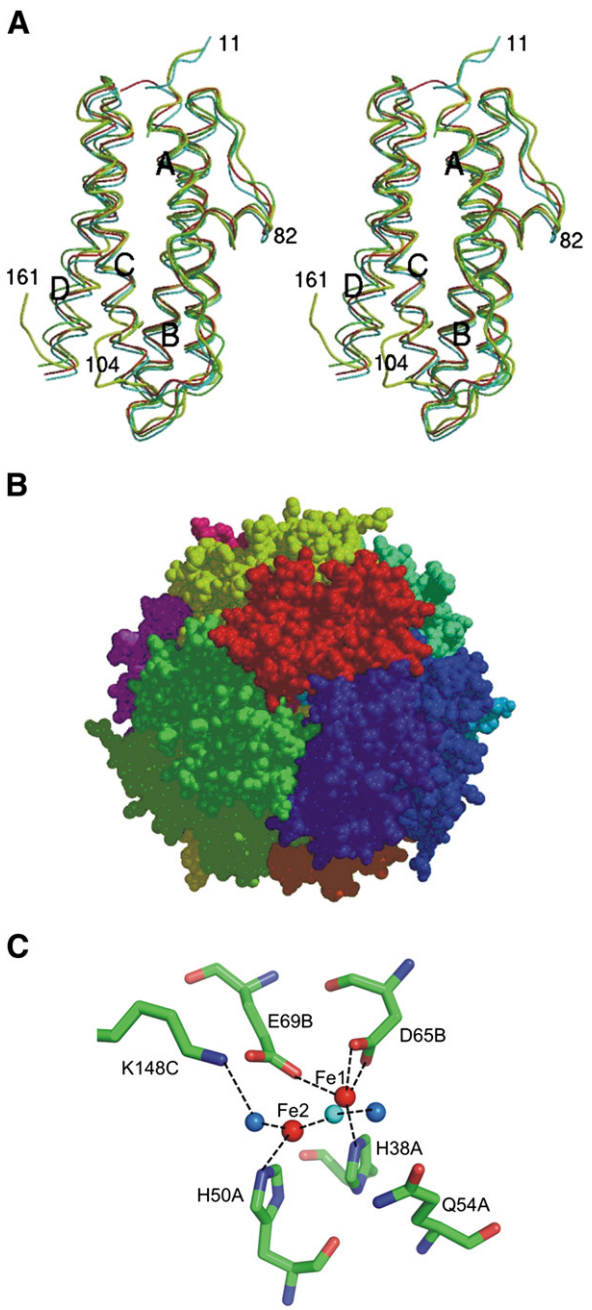


**Fig. 2.** Three-dimensional model of the NapA monomer and oligomer. (A) Superposition of Cα chain trace of monomer of NapA (yellow) to that of other proteins of the family: Dps from *Bacillus brevis* (blue, PDB code 1N1Q) [21], HP-NAP from *Helicobacter pylori* (green, PDB code 1JI4) [18], Dlp-2 from *Bacillus anthracis* (red, PDB code 1JIG) [17]. Residues are numbered according to [7]. (B) van der Waals representation of the NapA dodecamer. Each monomer is colored differently. One three-fold axis is running approximately perpendicular to the plane of the paper in the center of the image, through one of the putative tunnels for the iron entrance. (C) The Fe binding site. Two Fe ions (red) are coordinated by protein side chain residues and by solvent molecules (blue). The oxygen bridging the two Fe ions is shown in cyan (see text for more details).

### 3.2. Structure of the dodecamer

The quaternary organization of NapA is that of a dodecamer with a 23 symmetry. The macromolecular complex has a nearly spherical shape that tends to become a tetrahedron (Fig. 2B). The diameter of the assembly is more than 90 Å, with an internal cavity of about 50 Å. The dodecamer possesses four three-fold axes, each of them passing through the shell in two different three-fold environments. One of the two three-fold pores corresponds to the iron entry channel of Flp [20]. This pore has a definitely hydrophilic, negatively charged environment. From the outside to the inside, nine potentially negatively charged residues are conserved in all the proteins of this family. In NapA they are Asp 128, 140 and 141 and their symmetry mates. The other pore is only a virtual one, since it is closed by hydrophobic side chains, in particular Val 48.

### 3.3. The ferroxidase center

In the NapA dodecamer twelve cations binding sites are present, two per dimer. The relatively low resolution of our crystal does not allow a detailed description of this site. The electron density map is clear enough to allow us to state that two ions are present in each site, as in the case of *B. brevis* Dps structure [21]. Two Fe ions were refined in each site, along with two water molecules. One of the two irons presents a nearly tetrahedral coordination, given by Glu 69 and Asp 65 of one subunit, His 38 from another and a solvent molecule, whilst the second is coordinated to the same solvent molecule (the latter may be an oxygen, as assumed in Fig. 6 of Li et al. [7]), His 50 and a second water molecule. The latter is kept in place by Lys 148 (Fig. 2C).

### 3.4. N- and C-terminal tails of NapA are not crucial for its pro-Th17 activity

To verify whether the immunomodulating activity of NapA resides either in its N-terminal or in its C-terminal tail, we produced two NapA mutants lacking 13 residues at the N-terminus and 20 at the C-terminus, respectively, and assayed them for their Th17-orienting property. To this aim, monocytes isolated from healthy donors were

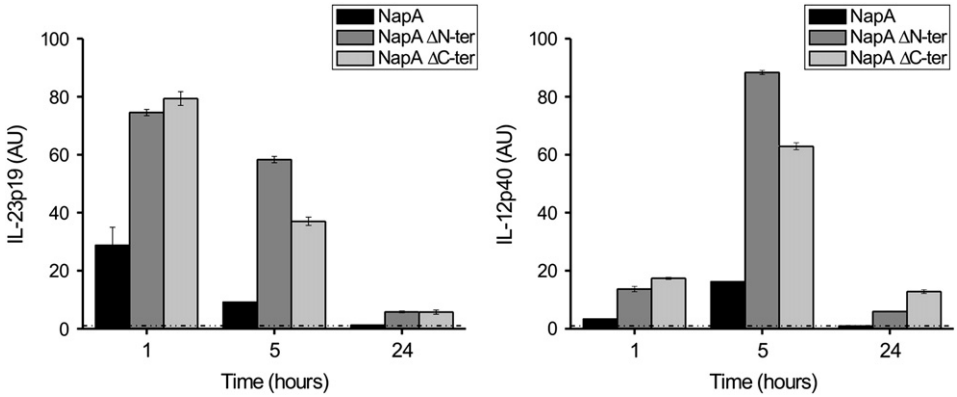


**Fig. 3.** Kinetics of IL-23 synthesis in monocytes stimulated with NapA wt and NapA deletion mutants. IL-23p19 and IL-12p40 cytokine mRNAs were quantified by real time PCR. The experiment shown is representative out of 4 experiments conducted with different cell preparations (AU, arbitrary units). The dotted lines represent the amount of cytokine mRNA produced by untreated cells.

incubated with NapA, either wt and deleted, and at different time points mRNA was extracted, retro-transcribed and amplified by real time PCR in the presence of primers specific for the cytokines crucial for the differentiation and expansion of Th17 cells, such as IL-23 (formed by the two subunits IL-23p19 and IL-12p40), IL-1β, IL-6 and TGF-β.

As expected, the amount of mRNA for both IL-12p40 and for IL-23p19 was increased in monocytes exposed to wt NapA with respect to untreated cells; surprisingly, the exposure to both the deleted forms of NapA resulted in an even more pronounced

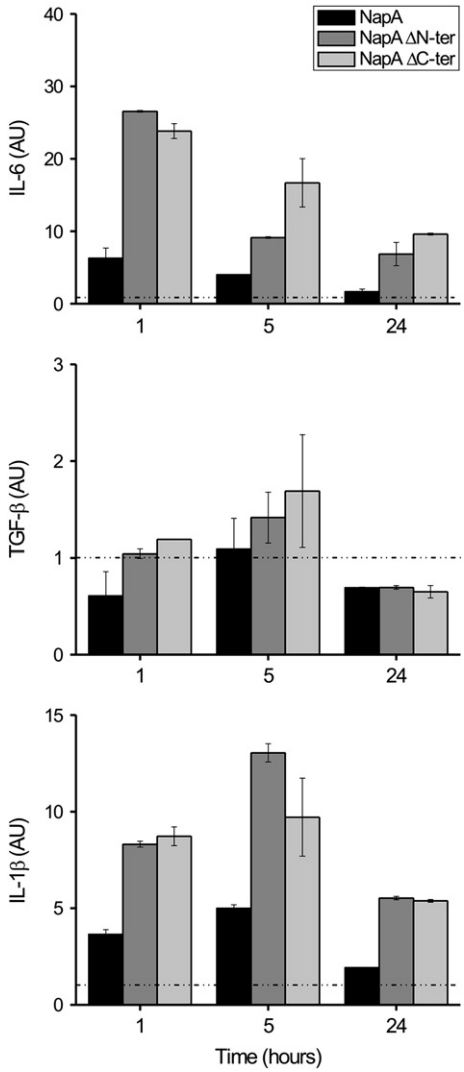


**Fig. 4.** Kinetics of IL-6, TGF-β and IL-1β synthesis in monocytes stimulated with NapA wt and NapA deletion mutants. Cytokines' mRNAs were quantified by real time PCR. The experiment shown is representative out of 4 experiments conducted with different cell preparations (AU, arbitrary units). The dotted lines represent the amount of cytokine mRNA produced by untreated cells.

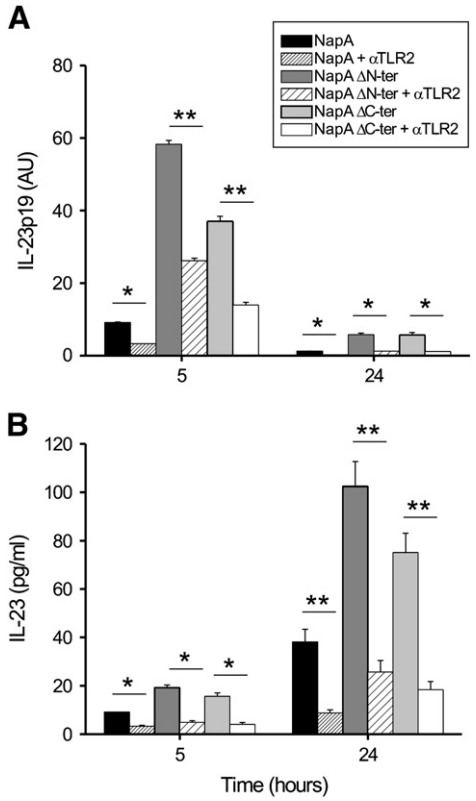


**Fig. 5.** The immunomodulatory properties of NapA deletion mutants occur through the engagement of TLR2. Monocytes were preincubated or not for 2 h with 20 μg/ml of an anti-TLR2 blocking antibody before being exposed to NapA wt or to NapA mutants. (A) After 5 and 24 h cells were harvested and mRNA levels of IL-23p19 quantified by real time PCR. The experiment shown is representative of three experiments conducted with different cell preparations (AU, arbitrary units). (B) The culture supernatants of the same cells (500 μl) were collected and an aliquot (100 μl) used for the ELISA evaluation of the secreted IL-23 cytokine. The not complete inhibition observed in the presence of the antibody is likely due to the not complete blockage of the receptor. Significance was determined by Student's t-test; *, $p<0.05$ and **, $0.01<p<0.05$ versus anti-TLR2 treated cells.

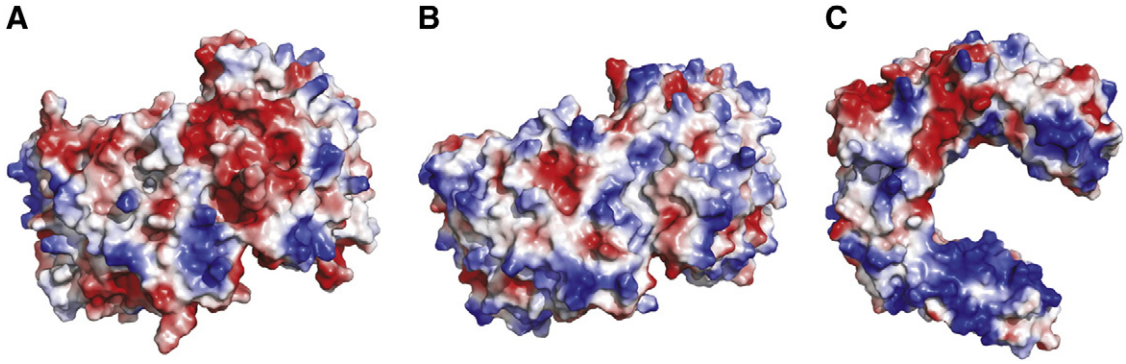


**Fig. 6.** Molecular surface of NapA (A), HP-NAP (B) and TLR2 (C) colored according to the Coulomb electrostatic potential (red, negative; blue, positive; minimum and maximum between −88 and +88 for A and B, from −60 to +60 for C). Only the tetramers of NapA and HP-NAP, oriented in the same way, are shown.

induction of mRNA for both IL-12p40 and IL-23p19 (Fig. 3). These results, suggesting that neither the N-terminus, nor the C-terminus of NapA were crucial for its immunomodulatory activity, were further confirmed by the evaluation of the IL-6, TGF-β and IL-1β mRNA (Fig. 4). Indeed, also in this case the deletion of the two NapA domains did not abrogate the ability of the protein to activate monocytes.

### 3.5. NapA mutants retain the ability to engage TLR2

Finally, to further investigate whether NapA mutants retain the ability to engage the TLR2, which is crucial for the immunomodulatory properties of the wild type protein [3], we evaluated the induction of IL-23 in the presence of a blocking anti-TLR2 antibody. As clearly depicted in Fig. 5 the presence of the antibody significantly reduced the ability of NapA, both wt and mutants, to promote the synthesis and release of IL-23, suggesting that the portion of the protein responsible for the binding to the receptor does not localize within the two N- and C-terminal tails.

## 4. Discussion

Both NapA from *B. burgdorferi* and HP-NAP from *H. pylori* have been demonstrated to be TLR2 agonists, despite displaying different effects in their immune response [3,16]. TLR2 plays a crucial role in innate immunity by recognizing several kinds of different microbial molecules, including lipoproteins, lipopolysaccharides, lipoteichioc acid, peptidoglycan and others [22]. A crucial step of TLR activation is represented by dimerization, either hetero or homo: as a consequence two TIR cytoplasmic domains become close enough to make them active to start the signal cascade [22]. The aspects of TLR2 activation have been dissected at the molecular level in the case of its interaction with lipopeptides: the two ester-bound lipid chains are inserted into an hydrophobic pocket of the extracellular region of TLR2, whilst the amide-bound lipid chain is inserted in an hydrophobic

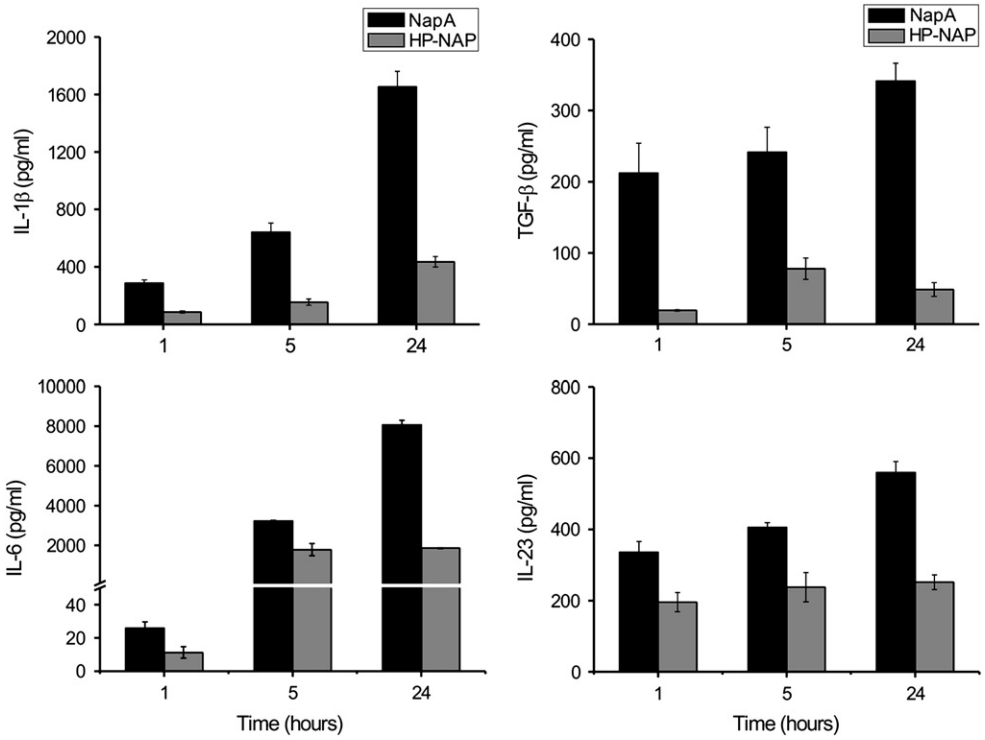


**Fig. 7.** NapA and HP-NAP differ in their ability to promote the secretion of pro-Th17 cytokines by monocytes. Monocytes isolated from healthy donors were incubated with 1 μM NapA or HP-NAP. At the indicated time points, supernatants were collected and the cytokines content was determined by specific ELISA kits.

channel of that of TLR1, inducing consequently the formation of an heterodimer TLR1–TLR2 [23]. Less clear is the mechanism of interaction of other possible ligands with TLR2, since most of them are molecules with chemical, conformational and electrostatic properties quite different from lipopeptides. Moreover, an interesting feature of the interaction of the TLR2 extracellular portions is that it is mainly hydrophilic, following the formation of several H-bonds [23].

It must be considered that the surface of NapA we present in this study lacks 13 residues at the N-terminus and 20 at the C-terminus, but both these domains are not involved in the interaction, as demonstrated by the fact that the deletion mutants retain their immunomodulatory properties as the wild type protein or even more. Consequently, the part of the external surface of our NapA model must contain the interaction site. The external surface of the extracellular region of TLR2 is quite hydrophilic, with a distribution of both positively and negatively charged amino acid side chains spread all around the surface. Something similar is true for both NapA and HP-NAP, whose exposed surfaces present a large number of negative and positive charges, the latter outnumbering the former [18]. It is consequently possible to hypothesize that NapA and HP-NAP directly interact with the extracellular region of TLR2 *via* polar and electrostatic interaction and, in doing so, they favor TLR2 dimerization in a way perhaps reminiscent to the dimerization of TLR4 mediated by *E. coli* MD-2 [24]. However, the charge distributions on NapA and HP-NAP are quite different (Fig. 6), making it hard to find a conserved area that could represent the surface of interaction with the receptor. This is in line with the evidence that the two bacterial proteins activate innate immune cells to secrete a different cytokine pattern, which, ultimately, triggers different adaptive immune responses: indeed, in a 24 h-incubation, the Th17 driving protein NapA stimulates monocytes to release 4 times more IL-1β, TGF-β and IL-6, and 2 times more IL-23, than HP-NAP (Fig. 7).This different activity could be the consequence of two different ways of interaction with TLR2.

## Acknowledgements

This work was supported by Progetto di Eccellenza Fondazione Cassa di Risparmio di Padova e Rovigo, Research Grant by University of Padova (CPDA074121/07), Associazione Italiana per la Ricerca sul Cancro Grant Regionale 2008, to M.d.B. The technical assistance of the staff of beamline XRD1 of the ELETTRA synchrotron (Trieste) during data collection is gratefully acknowledged.

## References

[1] R.A. Grant, D.J. Filman, S.E. Finkel, R. Kolter, J.M. Hogle, The crystal structure of Dps, a ferritin homolog that binds and protects DNA, Nat. Struct. Biol. 5 (1998) 294–303.
[2] C. Montecucco, M. de Bernard, Molecular and cellular mechanisms of action of the vacuolating cytotoxin (VacA) and neutrophil-activating protein (HP-NAP) virulence factors of *Helicobacter* pylori, Microbes Infect. 5 (2003) 715–721.
[3] G. Codolo, A. Amedei, A.C. Steere, E. Papinutto, A. Cappon, A. Polenghi, M. Benagiano, S.R. Paccani, V. Sambri, G. Del Prete, C.T. Baldari, G. Zanotti, C. Montecucco, M.M. D'Elios, M. de Bernard, *Borrelia burgdorferi* NapA-driven Th17 cell inflammation in lyme arthritis, Arthritis Rheum. 58 (2008) 3609–3617.
[4] M. de Bernard, M.M. D'Elios, The immune modulating activity of the *Helicobacter pylori* HP-NAP: friend or foe? Toxicon (2009).
[5] D.J. Evans Jr., D.G. Evans, T. Takemura, H. Nakano, H.C. Lampert, D.Y. Graham, D.N. Granger, P.R. Kvietys, Characterization of a *Helicobacter pylori* neutrophil-activating protein, Infect. Immun. 63 (1995) 2213–2220.
[6] M.M. D'Elios, A. Amedei, A. Cappon, G. Del Prete, M. de Bernard, The neutrophil-activating protein of *Helicobacter pylori* (HP-NAP) as an immune modulating agent, FEMS Immunol. Med. Microbiol. 50 (2007) 157–164.
[7] X. Li, U. Pal, N. Ramamoorthi, X. Liu, D.C. Desrosiers, C.H. Eggers, J.F. Anderson, J.D. Radolf, E. Fikrig, The Lyme disease agent *Borrelia burgdorferi* requires BB0690, a Dps homologue, to persist within ticks, Mol. Microbiol. 63 (2007) 694–710.
[8] C. Mueller, P. Hutter, R. Sahli, A. Bretz, L.N. Toutoungi, O. Peter, A mutagenic PCR identifies isolates of *Borrelia garinii* responsible for Lyme borreliosis, FEMS Microbiol. Lett. 191 (2000) 199–203.
[9] T.H. Bothwell, B. Mallett, The determination of iron in plasma or serum, Biochem. J. 59 (1955) 599–602.
[10] A.G. Leslie, The integration of macromolecular diffraction data, Acta Crystallogr. D Biol. Crystallogr. 62 (2006) 48–57.
[11] The CCP4 suite: programs for protein crystallography, Acta Crystallogr D Biol Crystallogr 50 (1994) 760–763.
[12] E. Gasteiger, A. Gattiker, C. Hoogland, I. Ivanyi, R.D. Appel, A. Bairoch, ExPASy: the proteomics server for in-depth protein knowledge and analysis, Nucleic Acids Res. 31 (2003) 3784–3788.
[13] A.T. Brunger, P.D. Adams, G.M. Clore, W.L. DeLano, P. Gros, R.W. Grosse-Kunstleve, J.S. Jiang, J. Kuszewski, M. Nilges, N.S. Pannu, R.J. Read, L.M. Rice, T. Simonson, G.L. Warren, Crystallography & NMR system: a new software suite for macromolecular structure determination, Acta Crystallogr. D Biol. Crystallogr. 54 (1998) 905–921.
[14] P. Emsley, K. Cowtan, Coot: model-building tools for molecular graphics, Acta Crystallogr. D Biol. Crystallogr. 60 (2004) 2126–2132.
[15] R.A. Laskowski, M.W. MacArthur, D.S. Moss, J.M. Thornton, PROCHECK: a program to check the stereochemical quality of protein structures, J. Appl. Crystallogr. 26 (1993) 283–291.
[16] A. Amedei, A. Cappon, G. Codolo, A. Cabrelle, A. Polenghi, M. Benagiano, E. Tasca, A. Azzurri, M.M. D'Elios, G. Del Prete, M. de Bernard, The neutrophil-activating protein of *Helicobacter pylori* promotes Th1 immune responses, J. Clin. Invest. 116 (2006) 1092–1101.
[17] E. Papinutto, W.G. Dundon, N. Pitulis, R. Battistutta, C. Montecucco, G. Zanotti, Structure of two iron-binding proteins from *Bacillus anthracis*, J. Biol. Chem. 277 (2002) 15093–15098.
[18] G. Zanotti, E. Papinutto, W. Dundon, R. Battistutta, M. Seveso, G. Giudice, R. Rappuoli, C. Montecucco, Structure of the neutrophil-activating protein from *Helicobacter pylori*, J. Mol. Biol. 323 (2002) 125–130.
[19] P. Ceci, A. Ilari, E. Falvo, E. Chiancone, The Dps protein of *Agrobacterium tumefaciens* does not bind to DNA but protects it toward oxidative cleavage: X-ray crystal structure, iron binding, and hydroxyl-radical scavenging properties, J. Biol. Chem. 278 (2003) 20319–20326.
[20] G. Bellapadrona, S. Stefanini, C. Zamparelli, E.C. Theil, E. Chiancone, Iron translocation into and out of *Listeria innocua* Dps and size distribution of the protein-enclosed nanomineral are modulated by the electrostatic gradient at the 3-fold "ferritin-like" pores, J. Biol. Chem. 284 (2009) 19101–19109.
[21] B. Ren, G. Tibbelin, T. Kajino, O. Asami, R. Ladenstein, The multi-layered structure of Dps with a novel di-nuclear ferroxidase center, J. Mol. Biol. 329 (2003) 467–477.
[22] S. Akira, K. Takeda, Toll-like receptor signalling, Nat. Rev. Immunol. 4 (2004) 499–511.
[23] M.S. Jin, S.E. Kim, J.Y. Heo, M.E. Lee, H.M. Kim, S.G. Paik, H. Lee, J.O. Lee, Crystal structure of the TLR1–TLR2 heterodimer induced by binding of a tri-acylated lipopeptide, Cell 130 (2007) 1071–1082.
[24] B.S. Park, D.H. Song, H.M. Kim, B.S. Choi, H. Lee, J.O. Lee, The structural basis of lipopolysaccharide recognition by the TLR4–MD-2 complex, Nature 458 (2009) 1191–1195.